

Random tilings of high symmetry: I. Mean-field theory

N. Destainville

Laboratoire de Physique Théorique, UMR CNRS-UPS 5152, Université Paul Sabatier, 31062 Toulouse Cedex 04, France.

M. Widom

Department of Physics, Carnegie Mellon University, Pittsburgh, PA 15213, USA.

R. Mosseri

Groupe de Physique des Solides, CNRS et Université 6, Campus Boucicaut, 140 Rue de Lourmel, 75015 Paris, France.

F. Bailly

LPSB-CNRS, 92195 Meudon Cedex, France.

(October 21, 2003)

We study random tiling models in the limit of high rotational symmetry. In this limit a mean-field theory yields reasonable predictions for the configurational entropy of free boundary rhombus tilings in two dimensions. We base our mean-field theory on an iterative tiling construction inspired by the work of de Bruijn. In addition to the entropy, we consider correlation functions, phason elasticity and the thermodynamic limit. Tilings of dimension other than two are considered briefly.

I. INTRODUCTION

The discovery of quasicrystals by Shechtman, *et al.*¹, and the proposal of Levine and Steinhardt² of their possible relationship with Penrose tilings³, motivated widespread investigation of tilings as models for quasicrystal structure. It is presumed that energetically favored atomic motifs form geometrical tiles, and that these tiles may be arranged quasiperiodically in space to describe the quasicrystal structure. We consider tiling models defined as projections from a higher D -dimensional lattice into a lower d -dimensional physical space. For example, 10-fold symmetric tilings may be projected from $D = 5$ into $d = 2$, and icosahedral tilings may be projected from $D = 6$ into $d = 3$. Figure 1 displays examples of tilings constructed as projections from D -dimensional simple cubic lattices into $d = 2$ -dimensional physical space. The difference between the higher dimension D and the tiling dimension d is called the *codimension*.

An important unsolved problem is understanding the interactions among tiles that may favor particular tile arrangements over others. The suggestion by Elser and Henley^{4,5} that random tilings spontaneously exhibit quasiperiodicity, created a subfield within the area of tiling theory. It was shown⁶, for at least one atomistic model quasicrystal^{6,7}, that quasicrystalline order emerges with random tiling, rather than Penrose-like, order. The best description for real quasicrystalline materials remains an open problem, depending whether one assumes that energetic interactions favor quasiperiodicity⁸ or that entropy stabilizes the quasicrystal structure at high temperatures^{5,6,9}.

In addition to their role in the theory of quasicrystals, random tiling models appear in a number of other interesting scientific contexts. Their combinatorial properties, for example their relationship to generalized partitions^{10–12} make them interesting models for study within pure mathematics^{13–20}. Some random tiling models provide examples of exactly solvable models^{21,22} of interest within statistical mechanics. We note a relationship with algorithms for sorting lists^{23,24}. Random tiling models have also been proposed as models for elastic membranes^{11,25}.

The random tiling theory of quasicrystals focuses on two important properties: The tiling entropy contributes to the configurational entropy of the quasicrystal, reducing its free energy and enhancing thermodynamic stability against other competing phases⁹; Variation of the entropy with average phason strain defines the phason elastic constants. Table I summarizes existing data on the configurational entropies of $d = 2$ rhombus tilings, showing a trend of monotonic increase with D . Table II shows corresponding data for $d = 3$ rhombohedron tilings.

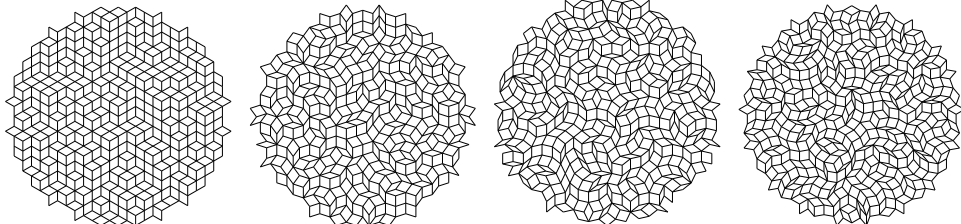


FIG. 1. Examples of free boundary $D \rightarrow 2$ tilings with $D = 3, 5, 7$ and 9 .

Techniques employed in theoretical studies include analytic exact solution²², Monte Carlo computer simulation²⁶ and numerical transfer matrix methods²⁷. While these methods prove successful at calculating quantitative values for entropy and elastic constants, they are not always easy to implement, and they often do not enhance our intuitive and qualitative understanding of the problem. The technique of mean-field theory²⁸ in statistical mechanics provides an approximation that can be analytically simple to implement and can provide a direct link between quantitative calculation and our qualitative picture of the physics of the problem. Mean-field theory often becomes exact in certain limits, such as the limit of infinite dimension. A mean-field theory for random tilings has never been precisely defined.

The search for an analogue of mean-field theory applicable to random tilings motivates our study of random tiling models with high rotational symmetry. We anticipate⁵ that the infinite D limit may prove easier to analyze than specific finite values of D . Experience gained in the study of this limit may later be transferred back to the finite D values of greatest physical interest. Furthermore, a study of D dependence of entropy or elastic constants might in itself yield qualitative understanding of the values of entropy and elastic constants for small D . Other researchers^{29–31} have studied deterministic quasiperiodic tilings of arbitrary rotational symmetry, but have considered neither the high symmetry limit nor the case of random tilings.

We mention, in addition, that high symmetry tilings are good candidates of models for topologically disordered graphs, different from the usual random graphs³² because the coordination number of a vertex is a random variable, with algebraically decreasing long-range correlations. Quantum diffusion on such tilings has recently been studied by Vidal *et al.* and was found to exhibit an interesting diffusive behavior³³. These tilings could even prove interesting as models for structural glasses.

Two previous papers^{24,34} presented initial studies of this problem. The first paper proposed an upper bound on the entropy in the limit of large D and discussed problems associated with the thermodynamic limit of tiling models. The second one³⁴ presented a preliminary mean-field approach of the entropy calculation. In the present paper we explain the previous work in greater detail. In addition, we inspect spatial correlations and phason elasticity. All tilings considered in this paper are free boundary tilings (see section II). Fixed boundary tilings are analyzed by computer simulation in the following paper³⁵. Table III summarizes the available estimates of the large D entropy.

The organization of this paper is as follows: We begin in section II with definitions and concepts that apply generally to random tiling models. Then, in section III we describe our mean-field theory of two-dimensional tilings of high rotational symmetry. We start with an upper bound (section III 1) then a more accurate estimate (section III 2) based on path counting arguments. We investigate the nature of spatial correlations in section III 3 followed by consideration on finite D corrections and phason elasticity. Tilings of dimension $d \neq 2$ are examined in section IV.

II. CHARACTERIZATION OF TILINGS

A tiling is a covering, without gaps or overlaps, of a given region of a d -dimensional Euclidean space. In the present paper, the tiles are d -dimensional rhombohedra, which we will generically call “rhombi” in the following.

Tiling systems can have different boundary conditions, such as free, fixed or periodic ones. For example, the tilings in figure 1 illustrate free boundary tilings of various rotational symmetries. The free boundary thermodynamic limit is taken as follows: Consider all tilings that cover a circular region of space \mathcal{R} (whose area will tend towards infinity). For a given \mathcal{R} , tilings contain fixed numbers of tiles of each type, with relative frequencies governed by the average composition of the tiling we wish to study. The total number of tiles is chosen so they encompass a total area slightly larger than area of the region \mathcal{R} that must be covered. Every tile must intersect \mathcal{R} or share an edge with a tile that does so. This ensures a reasonably compact tiling and gives us needed control over the composition.

It is generally supposed that free and periodic boundary tilings have the same entropies (provided their compositions match) at the thermodynamic limit. But fixed boundary tilings display a less usual behavior: such boundaries have such a macroscopic effect on tilings that their entropy per tile at the infinite size limit can be strictly smaller than the free boundary one. For example, in the case of “hexagonal” tilings of 60° rhombi ($D = 3$ and $d = 2$), when all orientations of rhombi occur with equal probability, the fixed boundary entropy per tile $\sigma_{fixed} = 0.261$ (³⁶) while the free boundary entropy per tile $\sigma_{free} = 0.323$ (³⁷). In addition to a qualitative argument by Elser³⁶, this phenomenon has more recently been rigorously explained and described^{38,17,18}: the local entropy can be calculated in any point of the tiling; it displays a gradient between the regions near the boundary, where the entropy is vanishing, and the central region, where the entropy is a free boundary one. In other words, it is only at the very center of the tiling that the tiling loses the influence of the boundary.

1. Membrane representation of tilings

Rhombic tiles can be considered as the projections onto a d -dimensional space of the d -dimensional faces of a hypercube in a space of higher dimension D . Conversely, any rhombic tiling in the d -dimensional space can be “lifted” to a d -dimensional continuous membrane embedded in the \mathbf{Z}^D hypercubic lattice. When this membrane is projected back into d -dimensional space, the facets of the D -dimensional lattice project precisely onto the d -dimensional rhombic tiles. Such a membrane is said to be *continuous* and *directed* to emphasize the fact that, when projected, it does not exhibit any gaps or overlaps. We say that we are dealing with $D \rightarrow d$ membranes or tilings. This *membrane* representation of rhombus tilings^{5,11,25,38} is a useful tool in quasicrystal science.

Notation related to the D -dimensional geometry and projection is described in appendix A. Let $(\hat{\mathbf{e}}_i)_{i=1,\dots,D}$ denote the basis of the \mathbf{Z}^D hypercubic lattice and denote by $\hat{\mathbf{e}}_i^\parallel$ the normalized projection of $\hat{\mathbf{e}}_i$ on the d -dimensional space where tilings lie. The projection direction is (arbitrarily) chosen so that the basis vectors $\hat{\mathbf{e}}_i^\parallel$ all have equal length and angles that are multiples of π/D (see appendix A). We call this collection of vectors a *regular fan*.

A rhombic tile has d edge orientations $\{\hat{\mathbf{e}}_i^\parallel, \hat{\mathbf{e}}_j^\parallel, \dots, \hat{\mathbf{e}}_k^\parallel\}$ with $(1 \leq i < j < \dots < k \leq D)$. We denote this tile species as $T_{ij\dots k}$. Note that there are $\binom{D}{d}$ different species of tiles. Examples of $D \rightarrow 2$ tilings are displayed in figure 1. The first one can be seen as a membrane embedded in a 3-dimensional cubic lattice, as may be more clear in the following figure 2.

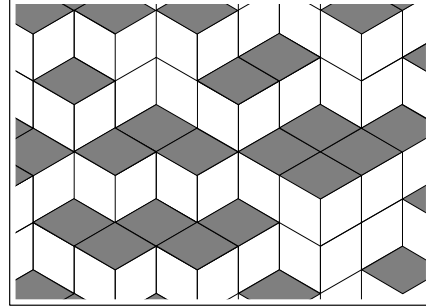


FIG. 2. Three-dimensional image effect. Gray rhombi can be seen as horizontal terraces.

Such random tilings have internal degrees of freedom, the so-called *localized phason flips*, which consist of local rearrangements of tiles. Such local flips are displayed in figure 3. In d dimensions, a flip involves $d + 1$ tiles that fill a small zonotope³⁹. Note that in 2 dimensions, the ergodicity of tiling ensembles *via* elementary flips is proven^{12,14}, whereas it is an open question in 3 and more dimensions. This local degree of freedom is the source of configurational entropy in random tilings.

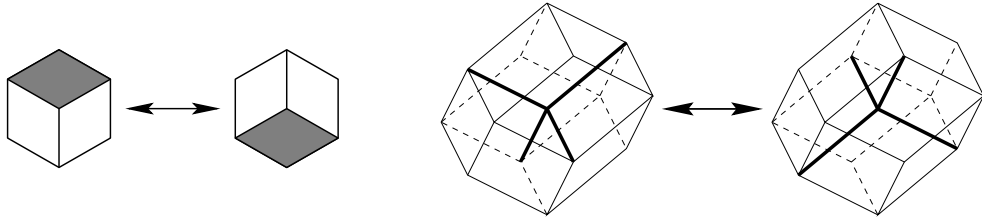


FIG. 3. Two examples of elementary flips in 2 and 3 dimensions, involving respectively 3 and 4 rhombic tiles.

A functional representation of these directed membranes will prove useful. Denote the d -dimensional “physical” or “real” space containing the actual tiles by $\mathcal{E}^\parallel = \mathbf{R}^d$, and the perpendicular $(D - d)$ -dimensional space by $\mathcal{E}^\perp = \mathbf{R}^{D-d}$. Since membranes representing tilings are directed, they are the graphs of single-valued continuous functions $h : \mathcal{E}^\parallel \rightarrow \mathcal{E}^\perp$. Such functions h are called the *height functions* of the corresponding tilings. The detailed construction of the spaces \mathcal{E}^\parallel and \mathcal{E}^\perp is described in appendix A when $d = 2$. Executing an elementary flip of vertex v changes the value of the height function locally at vertex v .

Since the membranes are embedded in a hypercubic lattice, they are irregular and faceted at on the length scale of individual tiles. The local height function h is usually coarse-grained to get a smoother function \bar{h} which closely tracks the local function h over long distances but which is nearly insensitive to individual single vertex flips^{5,11,40}. The function \bar{h} describes a smoothed membrane. Then one defines the *phason gradient* $\mathbf{E} = \nabla \bar{h}$. This $(D - d) \times d$ dimensional tensor controls the fractions of the different species of tiles.

The entropy can be written as a functional of the phason gradient⁵. Moreover, the random tiling model hypothesis states that this latter entropy has a unique maximum, corresponding to tile fractions maximizing the symmetry. The orientation of the real space \mathcal{E} is chosen so that the gradient is zero at this maximum, and the model states that the entropy density has a quadratic behavior near this maximum:

$$\sigma = \sigma_{\max} - \frac{1}{2} \nabla \bar{h} \cdot \mathbf{K} \cdot \nabla \bar{h} + o(|\nabla \bar{h}|^2). \quad (1)$$

By analogy with an usual elastic theory, the tensor \mathbf{K} is called the tensor of *phason elastic constants*.

The best known rhombus tilings of the plane is the Penrose³ tiling, which displays an exact quasiperiodicity. The membrane representation of a Penrose tiling is a flat, horizontal, sheet. The phason strain of this tiling vanishes. In addition, the Penrose tiling is virtually unique (up to translations) because it forbids localized phason flips. The random tiling hypothesis implies that the most typical tilings in a random tiling ensemble mimic the long-range order of the Penrose tiling, while enjoying the entropy of short-range fluctuations.

Random and perfect tilings with vanishing phason strain exhibit the highest symmetry consistent with the projection from $D \rightarrow d$. In two dimensions, this symmetry includes³¹ $2D$ -fold rotational symmetry. A given tiling itself generally has no point about which it is invariant under rotations, but two-point and higher correlation functions do exhibit the symmetry. In addition, there are two families of mirror symmetries, denoted “along” and “between” according to the relation between the mirror plane and the basis vectors $\hat{\mathbf{e}}_i^\parallel$.

2. De Bruijn dualization and iterative construction of tilings

The de Bruijn dualization⁴¹ provides another representation of random tilings. We present this technique in two dimensions and generalize it to higher dimensions when needed.

De Bruijn grids^{41–43} are made up of lines, the de Bruijn lines, that are sometimes called *worms*. These lines are made of adjacent tiles sharing an edge of given orientation. It is always possible to extend these lines through the whole tiling up to a boundary tile. An example is presented in figure 4. Since there are D different edge orientations, there are D different de Bruijn families. A rhombic tile corresponds to the intersection of two lines of different families. Hence there are $\binom{D}{2} = D(D - 1)/2$ tile species. There are no triple intersections, and lines of a same family never intersect, even in an infinite tiling, because no rhombus has four parallel edges.

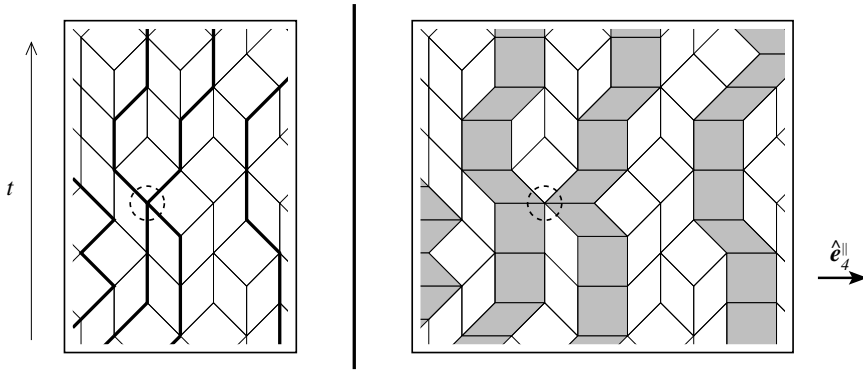


FIG. 4. Iterative process for the construction of $D \rightarrow 2$ tilings. Left shows paths on a re-oriented $3 \rightarrow 2$ tiling. Right shows the resulting $4 \rightarrow 2$ tiling. A non-crossing contact between two de Bruijn lines of the same family is emphasized.

This de Bruijn representation of tilings suggests an iterative construction of $D \rightarrow 2$ tilings in terms of directed random walkers on $D - 1 \rightarrow 2$ tilings. The basic idea is illustrated in figure 4. A $D - 1 \rightarrow 2$ tiling is sheared to make room for a new de Bruijn line family by taking the vectors $\hat{\mathbf{e}}_i^\parallel$ that initially lie at angles $\pi i / (D - 1)$ and replacing

them with angles $\pi i/D$ (see Fig. 4, left). Next, paths are chosen on the $D - 1 \rightarrow 2$ tiling (dark lines in Fig. 4, left). They go from bottom to top, as symbolized by a “time arrow” t . These paths must be “opened” in the direction $\hat{\mathbf{e}}_D^\parallel$ in order to form de Bruijn lines (shaded in Fig. (4) right) of the D -th family and therefore a $D \rightarrow 2$ tiling. These paths are directed in the positive time direction and they do not intersect within the same family. The figure shows a contact among paths that is not an intersection. Conversely, de Bruijn lines of family D in a $D \rightarrow 2$ tiling may be collapsed to directed walks in a $D - 1 \rightarrow 2$ tiling. There is thus a one-to-one correspondence between $D \rightarrow 2$ tilings with p de Bruijn lines of family D and collections of p non-intersecting walks on $D - 1 \rightarrow 2$ tilings.

3. Grid parameters, phason strain and tile fractions

1. Definitions

We now address two macroscopic characterizations of de Bruijn lines, the mean line spacings and orientations, and link these to the phason strain \mathbf{E} and the tile fractions n_{ij} (the fraction of tiles that are of type T_{ij}). De Bruijn lines of family i are characterized by the mean spacing l_i between two lines of the family i and the mean angle ϕ_i that lines of this family make with their nominal direction δ_i . The nominal direction (denoted by δ_i) is normal to $\hat{\mathbf{e}}_i^\parallel$ (see figure 5). For a maximally symmetric tiling with vanishing phason strain $\mathbf{E} = 0$, rotational symmetry guarantees that the mean line spacing l_i is independent of the line family i . We shall calculate its common value shortly. The strain-free tiling’s mirror symmetries guarantee that each angle $\phi_i = 0$. Deviations of l_i and ϕ_i from their strain-free values control nonzero values of \mathbf{E} and determine the tile fractions n_{ij} . By definition, $l_i > 0$ and $-\pi/2 < \phi_i < \pi/2$.

Figure 5 represents lines of the i -th family as sequences of tiles T_{ij} , each tile defined by the vector $\hat{\mathbf{e}}_j^\parallel$ and some other vector $\hat{\mathbf{e}}_j^\perp$. Let \mathbf{y}_0 be the relative position of a given tile in a de Bruijn line, and follow this line in the plane. The position $\mathbf{y}_m - \mathbf{y}_0$ of the m -th tile is the sum of the vectors defined by the successive edges of the tiles T_{ij} of the line between tile 0 and tile m . These vectors are *a priori* equal to $\pm\hat{\mathbf{e}}_j^\parallel$. Therefore we define $\mathbf{f}_j = \pm\hat{\mathbf{e}}_j^\parallel$ where the sign is chosen so that $\mathbf{f}_j \cdot \delta_i > 0$. For large m , the number of tiles T_{ij} on any typical line is proportional to the tile fraction n_{ij} . The mean direction of this line is therefore

$$\mathbf{d}_i = \sum_{\substack{j=1 \\ j \neq i}}^D n_{ij} \mathbf{f}_j. \quad (2)$$

In general, a random tiling ensemble is completely characterized by $\{l_i\}$ and $\{\phi_i\}$. Since $D - 2$ families of lines must be added to an original square lattice ($D = 2$) to define a $D \rightarrow 2$ tiling we need $2(D - 2)$ independent macroscopic parameters to characterize a tiling: l_i and ϕ_i for $i = 3, 4, \dots, D$. Note that $2(D - 2)$ is precisely the number of coefficients of the global phason gradient $\mathbf{E} = \nabla h$. By comparison, in reference [40], $4 \rightarrow 2$ tilings are characterized by 6 tile concentrations d_{ij} , and 2 exact relations constrain them. Therefore these tilings are characterized by 4 independent parameters, as predicted above.

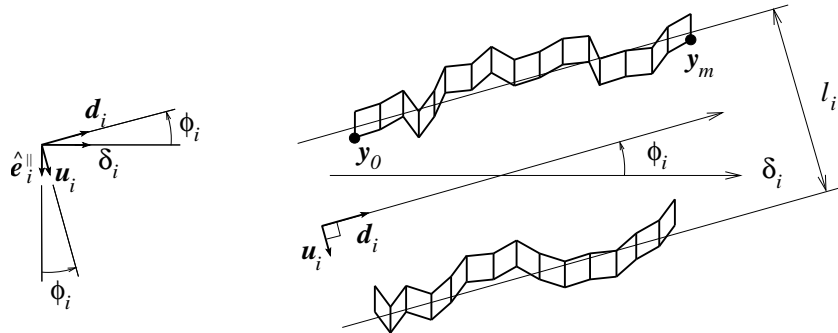


FIG. 5. Definition of quantities l_i – the mean distance between two neighbor lines of the i -th de Bruijn family – and ϕ_i – the mean angle that the lines of this family make with δ_i . The vector \mathbf{u}_i is given by the vector $\hat{\mathbf{e}}_i^\parallel$ rotated by the angle ϕ_i . The orientation \mathbf{d}_i of a line of the family i is given by the average of the vectors \mathbf{f}_j which define its tiles.

2. Relations

Consider now the tile fractions n_{ij} and their relation to $\{l_i\}$ and $\{\phi_i\}$. The tile number fractions n_{ij} are proportional to their density d_{ij} (number per unit area) via

$$n_{ij} = \frac{d_{ij}}{\sum_{k < l} d_{kl}}. \quad (3)$$

Conversely,

$$d_{ij} = \frac{n_{ij}}{\sum_{k < l} n_{kl} \sin |\pi(l - k)/D|} \quad (4)$$

because the area of a tile T_{ij} equals $\sin |\theta_{ij}^*|$ where $\theta_{ij}^* = \pi(j - i)/D$ is the oriented angle between $\hat{\mathbf{e}}_i^\parallel$ and $\hat{\mathbf{e}}_j^\parallel$.

Relation (3) is useful because the tile densities are given in a simple fashion by⁴⁰

$$d_{ij} = |\mathbf{m}_i \times \mathbf{m}_j|, \quad (5)$$

where \mathbf{m}_i (see appendix A) is the parallel space gradient of the i^{th} component of the smoothed membrane hyperspace coordinates. Examining figure 5, if one travels a distance l_i in the direction \mathbf{u}_i , then one crosses one de Bruijn line of the family i on average and the i^{th} component of the hyperspace coordinates increases by one on average. In contrast, if one travels any distance in the orthogonal direction \mathbf{d}_i , then the i^{th} component of the hyperspace coordinates remains constant. Thus

$$\mathbf{m}_i = \frac{1}{l_i} \mathbf{u}_i \quad (6)$$

and equation (5) becomes

$$d_{ij} = \frac{1}{l_i l_j} |\mathbf{u}_i \times \mathbf{u}_j| = \frac{1}{l_i l_j} |\sin \theta_{ij}|, \quad (7)$$

where the angle between de Bruijn line directions

$$\theta_{ij} = \theta_{ij}^* + \phi_j - \phi_i. \quad (8)$$

Next we relate the distances $\{l_i\}$ and angles $\{\phi_i\}$ to the phason strain \mathbf{E} . Owing to relation (A10) of appendix A, we have

$$\mathbf{E} = \sum_{i=1}^D \frac{1}{l_i} \hat{\mathbf{e}}_i^\perp \otimes \mathbf{u}_i. \quad (9)$$

Defining \mathbf{E}^2 as the sum of the squares of the components of \mathbf{E} , then

$$\mathbf{E}^2 = \sum_{i=1}^D \sum_{j=1}^D \frac{1}{l_i l_j} (\mathbf{u}_i \cdot \mathbf{u}_j) (\hat{\mathbf{e}}_i^\perp \cdot \hat{\mathbf{e}}_j^\perp). \quad (10)$$

We prove in appendix A that if $i \neq j$, then $\hat{\mathbf{e}}_i^\perp \cdot \hat{\mathbf{e}}_j^\perp = -2/(D-2) \cos \theta_{ij}^*$. Hence

$$\mathbf{E}^2 = -\frac{2}{D-2} \sum_{i \neq j} \frac{1}{l_i l_j} \cos \theta_{ij} \cos \theta_{ij}^* + \sum_i \frac{1}{l_i^2}. \quad (11)$$

To determine the tile fractions n_{ij}^* and the mean line spacing l_i^* for strain-free tilings (starred quantities will refer to unstrained tilings with $\mathbf{E} = 0$ throughout the text), recall that the tiling symmetry guarantees l_i is independent of i , and $\phi_i = 0$. Inspecting eqs. (7) and (3), we may write $n_{ij} = C |\sin \theta_{ij}^*|$. To determine the normalization constant C , note that

$$1 \equiv \sum_{i < j} n_{ij}^* = C \sum_{0 \leq i < j < D} \sin \pi \frac{j-i}{D}. \quad (12)$$

In the limit of large D one then finds $C \simeq \pi/D^2$, so that

$$n_{ij}^* = \frac{\pi}{D^2} |\sin \theta_{ij}^*|. \quad (13)$$

The fraction n_i of tiles belonging to a given family i of lines, in a maximally symmetric tiling at large D ,

$$n_i^* = \sum_{j \neq i} n_{ij}^* \simeq \frac{\pi}{D^2} \frac{2D}{\pi} = \frac{2}{D} \quad (14)$$

allows us to compute the mean distance between de Bruijn lines of a given family. Since tiles of family i have, on average, the same area as tiles of the whole tiling, the above *numerical* tile fraction is also an *area* tile fraction. Since a fraction $2/D$ of tiles belong to lines of a family and the width of such a line is 1, the mean distance between lines is

$$l_i^* = D/2. \quad (15)$$

Setting $l_i = l_i^*$ and $\theta_{ij} = \theta_{ij}^*$ for all i and j in (11), we find again in a consistent way $\mathbf{E}^2 = 0$. Moreover, eq. (7) implies

$$d_{ij}^* = \frac{4}{D^2} |\sin \theta_{ij}^*| = \frac{4}{\pi} n_{ij}^*. \quad (16)$$

3. Miscellaneous constraints

Geometrical considerations constrain the parameters $\{l_i\}$ and $\{\phi_i\}$. We describe a few such constraints here. The condition

$$\phi_{i-1} - \frac{\pi}{D} \leq \phi_i \leq \phi_{i+1} + \frac{\pi}{D} \quad (17)$$

imposes a certain regularity to the angles ϕ_i as a function of i . This constraint holds because lines of two consecutive families i and $i+1$ intersect only at a tile $T_{i,i+1}$, with edges $\hat{\mathbf{e}}_i^\parallel$ and $\hat{\mathbf{e}}_{i+1}^\parallel$ as displayed in figure 6. The oriented angles $(\mathbf{d}_i \mathbf{d}_{i+1})$ and $(\delta_i \delta_{i+1})$ have the same sign. Indeed, were these angles of opposite sign, no tile type could match at their intersection. As a consequence $(\mathbf{d}_i \mathbf{d}_{i+1}) = (\delta_i \delta_{i+1}) - \phi_i + \phi_{i+1} \geq 0$. Owing to $(\delta_i \delta_{i+1}) = \pi/D$, one gets $\phi_{i+1} - \phi_i \geq -\pi/D$ and condition (17) (see figure 6). Such conditions mean that at large D , when one adds a new family of lines in the iterative process, the angle ϕ_D is highly constrained by the pre-existing underlying tiling. For example, if a family $i = D$ is added in a strain-free tiling where $\phi_1 = \phi_{D-1} = 0$, the condition (17) reads $-\pi/D \leq \phi_D \leq \pi/D$.

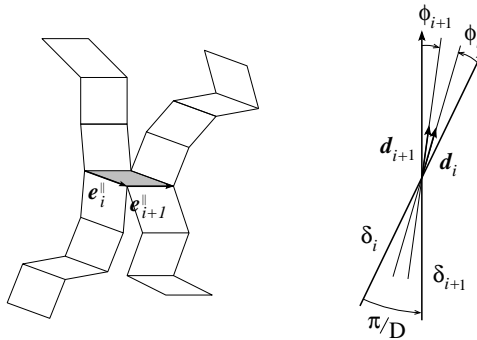


FIG. 6. Left: Intersection of two lines of two consecutive families i and $i+1$. Right: The corresponding directions δ_i , δ_{i+1} (outer thick lines) and \mathbf{d}_i , \mathbf{d}_{i+1} (inner thin lines). The vectors \mathbf{d}_i and \mathbf{d}_{i+1} are constrained by the condition $(\mathbf{d}_i \mathbf{d}_{i+1}) > 0$, which constrains in turn the angles ϕ_i and ϕ_{i+1} .

Since amongst the $2D$ parameters $\{l_i\}$ and $\{\phi_i\}$, only $2(D-2)$ are independent, there exist 4 relations between them. Of these four we will need this identity

$$\sum_{i < j} \frac{1}{l_i l_j} |\sin \theta_{ij}| |\sin \theta_{ij}^*| = 1. \quad (18)$$

which reflects the fact that the total contribution of tile areas per unit area is by definition equal to 1. In other words, $\sum_{i < j} d_{ij} |\sin \theta_{ij}^*| = 1$ where d_{ij} is given by eq. (7). This relation can also be derived from eq. (4).

In the large D limit we have infinitely many tile species, so we expect that all $n_{ij} \rightarrow 0$. When taking the large D limit we wish to ensure that no finite fraction of tile species dominates, with tile fractions that are large compared to the remainder. Indeed, such a tiling would essentially be a finite D tiling, with a negligible number of defect tiles added in. Thus we introduce the notion of “bounded” relative fractions of tiles, which proves useful in discussing large D phason elastic constants. Consider tilings in which all tile fractions tend to 0 as $D \rightarrow \infty$, all vanishing at the same rate. Specifically, assume there exists $a > 0$ such that

$$n_{ij} \geq a n_{ij}^* \quad (19)$$

holds uniformly for all i and j , which ensures that all tile fractions have the same order of magnitude as in strain-free tilings. Owing to eq. (4), we could alternatively assume that there exists $b > 0$ such that

$$d_{ij} \geq b d_{ij}^*. \quad (20)$$

Indeed, $\sum_{k < l} n_{kl} = 1$ thus $\sum_{k < l} n_{kl} \sin |\pi(l - k)/D| \leq 1$ and $d_{ij} \geq n_{ij}$. Furthermore $n_{ij} \geq a n_{ij}^* = \pi a / 4 d_{ij}^*$ and $b = \pi a / 4$.

In addition, conditions (19) or (20) constrain the distances l_i and the angles θ_{ij} so that

$$l_i \leq c l_i^* \quad (21)$$

where $c > 0$ is a finite constant, and

$$|\sin \theta_{ij}| \geq d |\sin \theta_{ij}^*| \quad (22)$$

with $d > 0$. Indeed, these two conditions together with eq. (7) imply $d_{ij} \geq (d/c^2) d_{ij}^*$.

Comparable constraints can be stated in the membrane viewpoint, in which case the constraints appear as extreme allowed values of \mathbf{E} . Using (11) and constraint (21), one finds that the phason strain is vanishingly small at large D ,

$$\mathbf{E}^2 \leq \frac{Cst.}{D}. \quad (23)$$

The only way to achieve finite strain at large D is to allow a finite subset of the tile species to dominate. This large D behavior is related to our choice of normalizations of basis vectors both in \mathcal{E}^\perp and in \mathcal{E}^\parallel . Our choice is consistent with current practice for finite D tilings.

4. Entropy loss due to contacts in strain-free tilings

An important feature of random tilings, which highly constraints their entropy, is the fact that de Bruijn lines of a same family cannot cross. In this subsection, we will characterize contacts between two lines.

We call “contact” between two neighbor lines of a same family a configuration where these lines are adjacent. Such a situation is represented in figure 4, where we have circled one contact between neighboring paths (or de Bruijn lines). If we follow the lines in the direction t , the local initial angles θ and θ' they make with their global direction δ after the contact are constrained by the noncrossing relation $\theta \leq \theta'$. This constraint divides the number of allowed configurations by a factor of order 2 as compared to the free path case, and reduces the total entropy by about $\log 2$.

To estimate the global entropy loss due to contacts in an infinite tiling, we must calculate the density of contacts. A crucial quantity is the distance L_i between consecutive contacts with neighboring lines of family i . Note that L_i depends on both l_i (because wider separation reduces the frequency of contacts) and ϕ_i (for subtle reasons described later in section III 5). In strain-free tilings, which have maximal rotational symmetry, $l_i = l_i^* = D/2$ and $\phi_i = 0$ and $L_i = L$ is independent of i .

Inspecting Fig. 4 we see that contacts between lines of family $i = D$ result from diffusion of the lines in the direction $\hat{\mathbf{e}}_D^\parallel$. Define the diffusion constant \mathcal{D} so that the lateral displacement u after traveling a distance L in the direction δ_i is $u^2 \sim \mathcal{D}L$. We presume that \mathcal{D} takes a finite limiting value in the large D limit. Thus $\mathcal{D}L \sim (l_i^*)^2$, and there is thus approximately one contact among lines of family i in every region of area $\mathcal{A} = l_i^* L = (l_i^*)^3 / \mathcal{D}$. Adding up the total number of contacts expected among lines of all orientations, we estimate the loss of entropy per unit area as

$$\Delta\sigma \approx -\frac{\mathcal{D}D}{(l_i^*)^3} \log 2 = -8\mathcal{D} \log 2 \frac{1}{D^2}. \quad (24)$$

This quantity should be suitably rescaled if one is interested in the entropy per tile. The strain-free loss of entropy falls off like $1/D^2$ because as D grows large, lines of like orientation rarely contact each other. We shall see in the forthcoming subsection III 5 that these calculations can be refined in the case of strained tilings, at least in a mean-field approximation.

III. MEAN-FIELD THEORY, CORRELATIONS AND FINITE D CORRECTIONS

This section applies the iterative construction of section II 2, to develop a mean-field theory of strain-free random tilings. We first propose a close upper-bound of $\log 2$ for the entropy per tile, which can be seen as the order 0 of the mean-field theory developed below. We then refine the estimate by calculating, within mean-field theory, the distribution of tile vertex types. Finally we explore spatial correlations and related issues.

1. First entropy estimate

Let $P_D(N_D)$ denote the number of ways to follow a directed walk of family D on a $D \rightarrow 2$ tiling. N_D is the total length of a single walk, or the cumulative length of a few walks. We will neglect contacts among walks of family D , which is justified since $l_i \sim D$. To calculate a typical value of $P_D(N_D)$, consider the problem of constructing bottom-to-top paths on a typical tiling. At each step, the path may follow one or more routes (Fig. 7). The only requirement is that the path segment leading out of a vertex must contain an upwards component. We estimate the number of paths as the product over vertices v of the number of choices $N_c(v)$ to be made at each step

$$P_D(N_D) \approx \prod_{v=1}^{N_D} N_c(v). \quad (25)$$

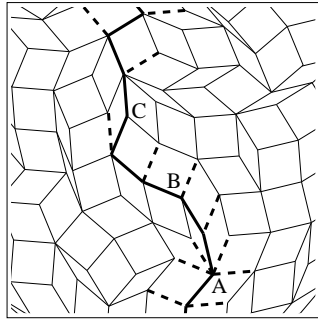


FIG. 7. A random path (thick line) on a tiling as a succession of vertices with choices (dashed edge = choice not taken). There are 5 choices at vertex A (*i.e.* $N_c(A) = 5$), 2 choices at vertex B and only 1 choice at vertex C.

Evaluation of equation (25) requires the distribution of values $N_c(v)$ along paths. Because we do not know this distribution (yet), we settle for an estimate that yields an upper bound on $P_D(N_D)$, and eventually on the entropy per tile S_D . Note that the product in equation (25) is the N_D -th power of the geometric mean of $N_c(v)$. The geometric mean of any set of positive numbers is bounded above by the arithmetic mean, reaching this bound only when all values are equal. The arithmetic mean $\bar{N}_c = \bar{Z}/2$, with \bar{Z} the mean coordination number (or degree), because on average half the tile edges at each vertex have a vertical component in the northerly direction. From Euler's theorem applied to infinite rhombus tilings, we know $\bar{Z} = 4$, so that $\bar{N}_c = 2$. We deduce the D -independent upper bound

$$P_D(N_D) \leq 2^{N_D}. \quad (26)$$

Let B_D be the number of $D \rightarrow 2$ tilings (free boundary tilings of some size \mathcal{R}). Since each $D + 1 \rightarrow 2$ tiling is in one-to-one correspondence with random walks on a $D \rightarrow 2$ tiling,

$$B_{D+1} \approx P_D(N_D)B_D. \quad (27)$$

We iterate this relationship to write

$$B_D = \prod_{D'=3}^{D-1} P_{D'}(N_{D'}) \quad (28)$$

Inserting relation (26) for the path counting, we find

$$B_D \leq 2^{N_3 + \dots + N_{D-1}}. \quad (29)$$

Since the number of tiles is $N = \sum_{D'} N_{D'}$, we obtain the entropy per tile

$$\sigma_D = \frac{\log B_D}{\sum N_{D'}} \leq \log 2 = 0.693. \quad (30)$$

The limiting entropy σ_∞ is bounded above by $\log 2$.

2. Refined mean-field calculations

The entropy value $\log 2$ just derived is not exact for two reasons. First, to properly compute the geometric mean of N_c we need the full vertex path choice probability distribution $\pi(N_c)$. Second, our estimate eq. (25) neglected correlations among the numbers of choices at different steps along the path. In this subsection we address the first point. In the conclusion we shall address briefly the second point.

Following the logic in section III 1, the limiting entropy is

$$\sigma_\infty = \lim_{D \rightarrow \infty} \lim_{k \rightarrow \infty} \frac{\log P_D(k)}{k}, \quad (31)$$

where $P_D(k)$ is the number of k -step paths on a $D \rightarrow 2$ tiling. The mean-field approximation assumes that the steps of such paths are uncorrelated so that the number of paths is given by eq. (25). The vertices v belong to a random $D \rightarrow 2$ tiling. Therefore the numbers of choices $N_c(v)$ are distributed according to a probability distribution $\pi_D(N_c)$. When D tends to infinity, this distribution tends toward a limiting distribution, denoted by $\pi(N_c)$. Thus, after a short calculation, equations (31) and (25) become:

$$\sigma_\infty^{MF} = \sum_{N_c=1}^{\infty} \pi(N_c) \log N_c. \quad (32)$$

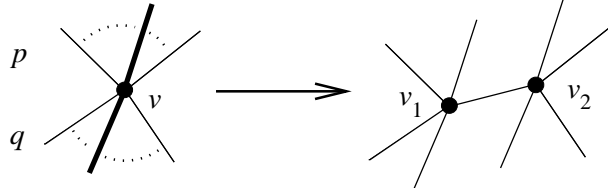


FIG. 8. A path going through a vertex v of a $D \rightarrow 2$ tiling gives birth to two vertices v_1 and v_2 of a $D + 1 \rightarrow 2$ tiling. The path follows any leg of v with probability $1/q$ and any arm with probability $1/p$.

To get the mean-field distribution $\pi(N_c)$, let us first denote by $\pi_D(q, p)$ the fraction of vertices on a $D \rightarrow 2$ random tiling with q in-coming edges (“legs”) and p out-going ones (“arms”) (see figure 8). Neglecting correlations, a (q, p) -vertex v of a $D \rightarrow 2$ tiling will be visited by paths with probability $\pi_D(q, p)$ and will then give birth to two vertices v_1 and v_2 , as illustrated in figure 8. These latter vertices belong to a $D + 1 \rightarrow 2$ tiling. Each leg and each arm of v will be chosen with probabilities $1/q$ and $1/p$, respectively. The new edge from v_1 to v_2 is arbitrarily chosen to be oriented upward in the $D + 1 \rightarrow 2$ tiling and is therefore an arm for v_1 and a leg for v_2 .

Indeed, a vertex with p' arms and q' legs can be either the “left-son” v_1 or the “right-son” v_2 of a “father-vertex” v in a $D \rightarrow 2$ tiling (figure 8). The two son vertices together inherit all their father’s arms and legs, plus an extra arm and leg (for the path along which the vertex is split). Finally, in addition, the left son gets an extra arm and the

right son an extra leg from the new bond that joins them. Consequently the left-son has more than one arm and the right-son has more than one leg.

As a consequence, in this mean-field approximation, the probabilities $\pi_{D+1}(q, p)$ can be written as linear combinations of the probabilities $\pi_D(q, p)$. The corresponding linear operator will be denoted by $\mathcal{A} : \pi_D \mapsto \pi_{D+1}$. It is infinite-dimensional since q and p can be arbitrarily large when D goes to infinity. The operator \mathcal{A} is defined by:

$$\pi_{D+1}(q', p') = (1 - \delta_{q', 1}) \sum_{\substack{q \geq q' - 1 \\ p \geq p'}} \frac{\pi_D(q, p)}{2qp} + (1 - \delta_{p', 1}) \sum_{\substack{p \geq p' - 1 \\ q \geq q'}} \frac{\pi_D(q, p)}{2qp}. \quad (33)$$

The first and second term refer, respectively, to left- and right-sons (v_1 and v_2). The factors of $1/2$ expresses that a vertex is either a left-son or a right-son with probability $1/2$. Moreover, each arm-leg pair is chosen with probability $1/pq$ among all possibilities (see figure 8). The limiting distribution $\pi(q, p)$ is the fixed point of \mathcal{A} , the eigenvector with eigenvalue 1.

The diagonalization of \mathcal{A} being rather complex, we focus on a summation of the previous relation on legs q . This yields a recursion relation on the arm statistics, in other words on the choice statistics

$$\pi_D(N_c) = \sum_{q=1}^{\infty} \pi_D(q, N_c). \quad (34)$$

We denote this operator by $\hat{\mathcal{A}}$ and write it in matrix form, where rows and columns are indexed by N_c , as

$$\hat{\mathcal{A}} = \begin{pmatrix} \frac{1}{2}1 & \frac{1}{2}\frac{1}{2} & \frac{1}{2}\frac{1}{3} & \frac{1}{2}\frac{1}{4} & \frac{1}{2}\frac{1}{5} & \cdots \\ \frac{1}{2}1 & \frac{1}{2} & \frac{1}{3} & \frac{1}{4} & \frac{1}{5} & \cdots \\ 0 & \frac{1}{2}\frac{1}{2} & \frac{1}{3} & \frac{1}{4} & \frac{1}{5} & \cdots \\ 0 & 0 & \frac{1}{2}\frac{1}{3} & \frac{1}{4} & \frac{1}{5} & \cdots \\ 0 & 0 & 0 & \frac{1}{2}\frac{1}{4} & \frac{1}{5} & \cdots \\ 0 & 0 & 0 & 0 & \frac{1}{2}\frac{1}{5} & \cdots \\ \vdots & \vdots & \vdots & \vdots & \ddots & \ddots \end{pmatrix}. \quad (35)$$

This operator preserves the mean number of choices $\langle N_c \rangle = 2$. The fixed point is

$$\pi(N_c) = \frac{1}{\sqrt{e}} \frac{2N_c - 1}{2^{N_c}(N_c - 1)!}. \quad (36)$$

The first few values of $\pi(N_c)$ are listed in table IV, where they may be compared with Monte Carlo simulation results (see paper II³⁵). The values peak at $N_c = 2$ and decrease rapidly for large N_c .

The mean-field entropy in eq. (32) becomes

$$\sigma_{\infty}^{MF} = \frac{1}{\sqrt{e}} \sum_{N_c=1}^{\infty} \frac{2N_c - 1}{2^{N_c}(N_c - 1)!} \log N_c \simeq 0.598. \quad (37)$$

This mean-field value is satisfactorily close to the numerical value obtained by Monte Carlo simulations (see paper II³⁵), namely $\sigma_{\infty} \simeq 0.568$, and is well below the upper bound $\log 2 = 0.693$.

3. Spatial correlations

Spatial correlations play a crucial role in two-dimensional finite codimension tilings since they are critical systems with long-range correlations²¹. In particular, they condition the diffusive behavior of de Bruijn lines, they constraint the successive steps in the iterative construction process, and they reduce the entropy slightly below the mean-field value. We can calculate both short- and long-range correlations within our mean-field theory.

Consider the short-ranged correlation between the numbers of arms and legs p and q on individual vertices. Within the mean-field approximation, $\langle pq \rangle_D = \sum_{p,q} \pi_D(q, p)pq$. If, at step D , a vertex v has p arms and q legs (see Fig. 8), then its first son v_1 has on average $(2 + 3 + \dots + (p + 1))/p = (p + 3)/2$ arms independently of its number of legs, and

$(1 + \dots + q)/q = (q+1)/2$ legs independently of its number of arms. Similarly, its second son v_2 has on average $(p+1)/2$ arms and $(q+3)/2$ legs. Therefore

$$\begin{aligned} \langle pq \rangle_{D+1} &= \sum_{p,q} \pi_D(q,p) \left(\frac{1}{2} \frac{p+1}{2} \frac{q+3}{2} + \frac{1}{2} \frac{p+3}{2} \frac{q+1}{2} \right) \\ &= \frac{1}{4} (\langle pq \rangle_D + 11), \end{aligned} \quad (38)$$

since $\langle p \rangle_D = \langle q \rangle_D = \langle N_c \rangle_D = 2$. The limiting value is $\langle pq \rangle_\infty = 11/3$. Moreover, distribution (36) leads to $\Delta p = (\langle p^2 \rangle_\infty - \langle p \rangle_\infty^2)^{1/2} = \sqrt{3}/2$ and $\Delta p = \Delta q$. Therefore the mean-field covariance of p 's and q 's is

$$\text{cov}(p, q) = \frac{\langle pq \rangle_\infty - \langle p \rangle_\infty \langle q \rangle_\infty}{\Delta p \Delta q} = -4/9 \simeq -0.44, \quad (39)$$

also in good agreement with the numerical value $\text{cov}(p, q) \simeq -0.36$ (see paper II³⁵). The main contribution to those correlations comes from the asymmetry caused by the edge between v_1 and v_2 .

To calculate long-range correlations using our iterative construction method, two phenomena compete: de Bruijn lines running through a tiling destroy vertex-to-vertex correlations, while they increase distances between vertices. Consider two vertices separated by a distance u_n on an $n \rightarrow 2$ tiling. The addition of successive families of lines to get higher codimension tilings ($D \rightarrow 2$ with $D > n$) make the tiling “swell” homogeneously, and the distances grow like D . When D increases, the distance between the two vertices increases so that

$$u_D/D \simeq u_n/n. \quad (40)$$

The idea is now to track such pairs of vertices, and to estimate how their correlation functions evolve at the same time they are moving apart.

To track these correlation functions as D increases, we estimate correlations between the number of choices at vertices, $N_c(v)$. Define the correlation function between vertices v_a and v_b , widely separated in space,

$$C_n(r) = \frac{1}{N_P} \sum_{d(v_a, v_b)=r} N_c(v_a) N_c(v_b) - \left(\frac{1}{N_v} \sum_v N_c(v) \right)^2 = \langle N_c(v_a) N_c(v_b) \rangle_r - \langle N_c \rangle^2. \quad (41)$$

The first average runs over the N_P pairs of vertices of $n \rightarrow 2$ tilings separated by a distance r . The second average runs over all N_v vertices in the tiling. In the following, we denote $\langle N_c(v_a) N_c(v_b) \rangle_r = \gamma_n$. Moreover the mean number of choices $\langle N_c \rangle = 2$, so that

$$C_n(r) = \gamma_n - 4. \quad (42)$$

When a new line passes through either v_a or v_b , their correlation diminishes. Each vertex has a probability $2/n$ that a new line goes through it (see eq. (14)). Therefore the probability that either one of the pair (v_a, v_b) will be affected by a new line is $4/n$. A fraction $1 - 4/n$ of pairs separated by r are unaffected, so their correlation remains equal to γ_n . The remaining pairs are affected, and we denote their new correlation by γ'_n which we now calculate.

Each pair (v_a, v_b) that is affected gives birth to two pairs. One of its vertices, say v_b , remains unchanged while the other one, v_a , gives birth to two vertices, a “left-son” v_{a1} and a “right-son” v_{a2} (see Fig. 8). On average,

$$N_c(v_{a1}) = \frac{1 + 2 + \dots + N_c(v_a)}{N_c(v_a)} = N_c(v_a)/2 + 1/2, \quad (43)$$

and $N_c(v_{a2}) = N_c(v_a)/2 + 3/2$, since a right-son has one more arm than a left-son. Therefore, averaging on the whole tiling, we find

$$\gamma'_n = 1/2 (\langle N_c(v_{a1}) N_c(v_b) \rangle + \langle N_c(v_{a2}) N_c(v_b) \rangle) = \gamma_n/2 + 2. \quad (44)$$

Now we estimate γ_{n+1} , the correlation averaged over all tiling vertices after the introduction of the lines of family $n+1$. For original vertices *not* touched by the new lines, the correlation remains γ_n . For original vertices that *are* touched by the new lines, the correlation becomes γ'_n . Therefore,

$$\gamma_{n+1} = \frac{(1 - 4/n)\gamma_n + 8/n \gamma'_n}{(1 - 4/n) + 8/n} \approx (1 - 8/n)\gamma_n + 8/n \gamma'_n + \mathcal{O}(1/n). \quad (45)$$

Hence

$$C_{n+1}(u_{n+1}) = (1 - 4/n)C_n(u_n). \quad (46)$$

Now iterating from $n \rightarrow D$ we write

$$C_D(u_D) = C_n(u_n) \prod_{k=n+1}^D (1 - 4/k). \quad (47)$$

For large n and D ,

$$\log C_D = \log C_n + \sum_{k=n}^{D-1} \log(1 - 4/k) \simeq \log C_n - 4 \sum_{k=n}^{D-1} 1/k \simeq \log C_n - 4 \log(D/n) \quad (48)$$

from which it follows that

$$D^4 C_D(u_D) \simeq n^4 C_n(u_n). \quad (49)$$

Using eq. (40) we have

$$(u_D)^4 C_D(u_D) \simeq (u_n)^4 C_n(u_n). \quad (50)$$

and finally

$$C_\infty(r) \simeq C \text{st. } \frac{1}{r^4}. \quad (51)$$

This expression holds only for large values of r , since we do not take into account the discreteness of tilings at very short range. Correlations fall off rapidly at large distance.

4. Finite D corrections

The mean-field calculations of section III 2 neglect the fact that at the step D of the iterative process, only a diminishing fraction of the vertices are visited by paths. Correcting this oversight does not alter the fixed point of the process, but predicts finite D corrections to it. Indeed, at step D , a fraction $2/D$ of the vertices are visited. Each of them has 2 sons and equation (33) applies only to a fraction of new vertices of order $4/D$ when one iterates at step D . The remaining vertices are unaffected. Hence the correct evolution operator is

$$\hat{\mathcal{A}}_D = \frac{4}{D} \hat{\mathcal{A}} + \left(1 - \frac{4}{D}\right) \text{Id.} \quad (52)$$

where $\hat{\mathcal{A}}$ is the operator introduced in eq. (35). For any finite D , the fixed point of $\hat{\mathcal{A}}$ remains the fixed point of $\hat{\mathcal{A}}_D$. Any eigenvector e of $\hat{\mathcal{A}}$ associated with the eigenvalue μ evolves as follows:

$$\hat{\mathcal{A}}_D \hat{\mathcal{A}}_{D-1} \dots \hat{\mathcal{A}}_2 \cdot e = \prod_{k=2}^D \left(\frac{4}{k} \mu + \left(1 - \frac{4}{k}\right) \right) e = \prod_{k=2}^D \left(1 + \frac{4(\mu-1)}{k} \right) e \simeq \frac{C}{D^{4(1-\mu)}} e, \quad (53)$$

where C is some constant of order 1, using the same calculation scheme as in equations (48) and (49).

Hence we get power-law convergence towards the fixed point instead of exponential convergence. The spectrum of $\hat{\mathcal{A}}$ can be calculated numerically, by taking finite but larger and larger approximations of \mathcal{A} . The spectrum converges rapidly towards $\{1, 1/2, 1/3, \dots, 1/p, \dots\}$. Eigenvalue $\mu = 1$ is the desired fixed point. The slowest mode corresponds to $\mu = 1/2$ and to a $1/D^2$ behavior of the finite D corrections to $\pi(N_c)$, and therefore to the entropy (32). Thus finite D corrections to the entropy associated with path-counting are expected to behave like $1/D^2$ in the mean-field approximation. As compared to corrections (also of order $1/D^2$) due to contacts and related to large-scale diffusive properties, the latter corrections take into account the local structure of tilings via the distribution of numbers of choices.

The previous entropy is an entropy per tile concerning the tiles of the new D -th family. However we shall see that the corrections to the entropy per tile of the *whole* tiling differ slightly from the above corrections and are of order $(\log D)/D^2$. The finite D entropy per tile σ_D satisfies the recurrence relation

$$\sigma_D = \left(1 - \frac{2}{D}\right) \sigma_{D-1} + \frac{2}{D} \left(\sigma_\infty + \frac{A}{D^2}\right), \quad (54)$$

because a fraction $1 - 2/D$ of tiles belong to the underlying $(D-1) \rightarrow 2$ tiling, the entropy per tile of which is σ_{D-1} , while the remaining tiles belong to the de Bruijn lines added to this underlying tiling. Their entropy per tile is therefore σ_∞ plus the finite D corrections of order $1/D^2$, as discussed above. If we define $\sigma_D = \sigma_\infty + \varepsilon_D$, we get

$$\varepsilon_D = \frac{D-2}{D} \varepsilon_{D-1} + \frac{2A}{D^3} \quad (55)$$

thus

$$D(D-1) \varepsilon_D = (D-1)(D-2) \varepsilon_{D-1} + 2A \frac{D-1}{D^2}, \quad (56)$$

from which it follows that $D(D-1)\varepsilon_D \sim 2A \log D$ and

$$\sigma_D = \sigma_\infty + 2A \frac{\log D}{D^2}. \quad (57)$$

This point deserves a short discussion: the rough argument of section II 4 was based on the fact that all de Bruijn lines play the same role. However, to be more precise, families of lines are added one after the other. That is to say the effects of finite-size corrections due to one family must be taken into account before adding the next family. The D -th family is added on a real $(D-1) \rightarrow 2$ tiling, on which it must already be taken into account that de Bruijn lines cannot intersect.

5. Phason elastic constant tensor

The entropy considered so far, in particular its finite size corrections, only concerned maximally symmetric tilings, without phason strain. A central claim of random tiling theory is that the entropy is maximized in the absence of global phason strain, and varies quadratically around this maximum. Then the entropy satisfies

$$\sigma_D(\mathbf{E}) \simeq \sigma_{\max} - \frac{1}{2} \mathbf{E} \cdot \mathbf{K} \cdot \mathbf{E} \quad (58)$$

where $\sigma_{\max} = \sigma_D$. We can test this claim in the context of mean-field theory and reach insight into the properties of the phason elastic constant tensor \mathbf{K} . In particular, we shall see that these constants decay like $\log D/D$ when D becomes large. As discussed previously, two kinds of corrections to the limiting value of the entropy occur for finite values of D . We must determine how these two influences on the entropy are affected by phason strain.

On the one hand, in section II 4, one mechanism by which phason strain influences the entropy is through the non-crossing rule for like-oriented paths in our iterative tiling construction. Every time two like-oriented paths contact each other we lose approximately $\log 2$ in entropy due to the non-crossing constraint. The frequency of contacts depends upon the phason strain through the parameters l_i and ϕ_i . On the other hand, the mean-field entropy, as expressed in eq. (32), will certainly be affected if the iterative equations are biased by parameters ϕ_i or l_i deviating from their strain-free values.

To estimate the strain-dependence of the loss of entropy by contact we must calculate the density of contacts as a function of strain. To begin with, we impose a global phason strain by varying only the mean distance l_i between de Bruijn lines of family i . Let

$$l_i = l_i^*(1 + \lambda \delta_i) \quad (59)$$

where λ is a small parameter that controls the strength of the phason strain. Here δ_i is an arbitrary but bounded function of i whose mean and standard deviation obey $\langle \delta \rangle = 0$ and $\langle \delta^2 \rangle = 1$, where the averages are taken over families i . Note that owing to the bounded tile fraction constraint eq. (21), whatever the strength of the phason strain, l_i is of order D and λ is of order at most 1.

The condition $\langle \delta \rangle = 0$ comes from the normalization (18), rewritten as

$$\sum_{i,j} \frac{1}{l_i l_j} |\sin \theta_{ij}| |\sin \theta_{ij}^*| = 2 \quad (60)$$

expanded to first order in λ and ϕ_i . The term of first order in λ on the left hand side multiplies $\sum \delta_i$, hence this sum must vanish.

Consider a pair of adjacent lines of family i , and evaluate L_i , the mean distance between contacts of these lines. Thus $\mathcal{D}L_i \sim l_i^2$, and there is thus approximately one contact among lines of family i in every region of area $\mathcal{A}_i = l_i L_i = l_i^3 / D$. The entropy loss (24) becomes

$$\Delta\sigma \approx -\mathcal{D}D < l^{-3} > \log 2. \quad (61)$$

Now consider the average $< l^{-3} >$. For vanishing phason strain ($\lambda \rightarrow 0$), eq. (15) reveals that $l_i = l_i^* = D/2$. Expanding l_i^{-3} in eq. (59) for small λ , using the known mean and standard deviation of δ_i , we obtain

$$< l^{-3} > \approx \left(\frac{2}{D} \right)^3 (1 + 3\lambda^2). \quad (62)$$

Substituting this expression into eq. (61) yields

$$\Delta\sigma \approx - \left(\frac{1}{D^2} + \frac{3\lambda^2}{D^2} \right) 8\mathcal{D} \log 2. \quad (63)$$

We find two terms, each falling off as $1/D^2$. The first term is independent of the phason strain magnitude λ and is of order $1/D^2$, because lines of like orientation, which are forbidden to cross, rarely contact each other. In a strained tiling with $\lambda \neq 0$, owing to eq. (21), l_i remains of order D , and the loss of entropy is also of order $1/D^2$. Although the frequency of contacts increases due to the strain, it still falls off for large D .

Should the angles ϕ_i be non vanishing, we would reach the same conclusion, since the distance between de Bruijn lines would remain of order D . Likewise, variation of the diffusion constant \mathcal{D} with respect to l_i and ϕ_i will be small as compared to \mathcal{D} itself, and the corrections to the entropy will remain of order $1/D^2$.

As far as the mean-field contribution to the finite D entropy, corrections is concerned, we now reexamine the argument of section III 4 for strained tilings. Our mean-field theory does not allow us to estimate the effects of angles ϕ_i because the splitting process of section III 2 does not keep track of edge orientations. Introduction of finite angles ϕ_i at any stage of the iterative process biases the operator (33), since if the path prefers, say, a left orientation (*i.e.* $\phi_{D+1} > 0$), right sons v_2 have more arms than left ones v_1 . Calculation of this bias would require a much more complicated operator than we have used thus far.

By contrast, we can incorporate the strain induced by line separations l_i . Setting $l_k = l_k^*(1 + \lambda\delta_k)$, taking account the “swelling” effect described in III 3, when this k -th de Bruijn family is introduced at stage k of the iterative process its actual line separation is $l'_k = (k/2)(1 + \lambda\delta_k)$. The fraction of vertices visited by this k -th line is

$$\frac{1}{l'_k} = \frac{2}{k}(1 + \lambda\hat{\delta}_k), \quad (64)$$

instead of $2/k$. Expanding $\hat{\delta}_k$ in Fourier modes, we set $\hat{\delta}_k = a_0 \exp(i(2\pi k/k_0 + \psi))$ to describe a single mode of “wavelength” k_0 . Equation (53) becomes

$$\hat{\mathcal{A}}_D \hat{\mathcal{A}}_{D-1} \dots \hat{\mathcal{A}}_2 \cdot e = \prod_{k=2}^D \left(1 + \frac{4(\mu-1)}{k} \left(1 + \lambda a_0 e^{i(2\pi k/k_0 + \psi)} \right) \right) e \simeq \frac{C'(\lambda)}{D^{4(1-\mu)}} e. \quad (65)$$

This result differs from eq. (53) because C' is a function of λ . Of course, $C'(\lambda=0)$ equals the value of C in eq. (53). To find out how C' depends on λ , take the logarithm of the product in eq. (65) and consider the first order term in λ as an example. Since

$$\lambda a_0 \sum_{k=1}^{\infty} \frac{e^{i(ak+\psi)}}{k} = -\lambda a_0 e^{i\psi} \log(1 - e^{ia}), \quad (66)$$

is of order 1, it appears that $C'(\lambda)$ is a decently behaved function. In particular, C' remains of order 1. Consequently, phason corrections to the entropy density of the whole tiling remain of order $\log D/D^2$ as discussed in section III 4.

In contrast to eq. (63), the effect is first order in λ , because we examine here a specific realization of phason strain where previously the phason strain was fluctuating.

Because the entropy is independent of the phason strain, we again conclude that the phason elastic constant vanishes. We have seen (eq. (23)) that for bounded tile fractions the phason strain \mathbf{E}^2 decreases like $1/D$ as D increases. Comparing eq. (58) with our strain-corrections of order $\log D/D^2$, we might conclude that the phason elastic tensor \mathbf{K} falls off as $\log D/D$. However, recall that the order λ^1 term reflects the use of just a single, special phason strain whose funny D -dependence may be responsible also for the appearance of the $\log D$. It is probable that the contribution to the phason elastic constant associated with line tilt truly falls off just as $1/D$.

We can understand the vanishing phason strain correction by the following qualitative argument. Consider a domain of the tiling of diameter Δ , large as compared to the tile size 1 but small as compared to the mean distance between two lines of a same family, $1 \ll \Delta \ll D$. For example, one can choose $\Delta = \sqrt{D}$. In such a domain there is *at most* one de Bruijn line per family, and no lines at all of most families. Since Δ tends to infinity with D , the area of the domain tends to infinity and the number of lines and tiles in the domain also tend to infinity.

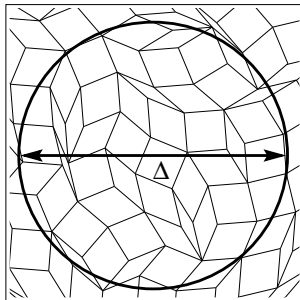


FIG. 9. A domain of diameter Δ which contains at most one de Bruijn line per family.

Locally, as D and Δ go to infinity, the tiling looks like a large codimension $D' \rightarrow 2$ tiling (where $D' \sim \Delta$), with only one line per family (see Fig. 9). The entropy per tile in this domain tends towards a quantity σ_{loc} which depends neither on the strain nor on the domain under consideration and is directly related to a simplified problem with one line in each family. The global entropy per tile σ_∞ is the average over the whole tiling¹¹ of the local entropy σ_{loc} . Therefore $\sigma_\infty = \sigma_{loc}$ is independent of the de Bruijn line separations l_i , of the angles ϕ_i and of the global phason strain.

IV. TILINGS OF DIMENSION OTHER THAN 2

This section discusses briefly cases of dimension other than $d = 2$. The high codimension $d = 1$ case is especially interesting because it is exactly solvable. It serves as an excellent illustration of several of the concepts in the paper and contrasts interestingly with the high codimension $d = 2$ case. We then present results and conjectures for the high codimension $d = 3$ case and the codimension 1 case with $d = D - 1$ for arbitrary d .

1. $D \rightarrow 1$ tilings

One-dimensional high codimension $D \rightarrow 1$ tilings are exactly solvable. These tilings comprise D different species of tiles randomly arranged on a line. This case is unusual since the entropy per tile tends to infinity with D . Still, this example is quite instructive since it already contains a characteristic feature of large codimension tilings: when D goes to infinity, we prove that the entropy no longer depends on the relative tile fractions provided these quantities remain bounded.

The number of tilings is given by the multinomial coefficient:

$$W^{D \rightarrow 1}(k_1, \dots, k_D) = \frac{(k_1 + k_2 + \dots + k_D)!}{k_1! k_2! \dots k_D!}. \quad (67)$$

Introducing tile fractions $x_i = k_i/(k_1 + \dots + k_D)$, we get the entropy per tile at large D

$$\sigma^{D \rightarrow 1} = - \sum_{i=1}^D x_i \log x_i. \quad (68)$$

This entropy is maximal at $x_i = 1/D$ where it equals $\log D$. In one dimension, for the sake of convenience in the calculation, we set the upper bound $x_i \leq a/D$ where $a > 0$ to prevent some tile species from being dominant. Then $-\log x_i \geq \log D - \log a$, and hence $-\sum_{i=1}^D x_i \log x_i \geq \log D - \log a$ because $\sum_{i=1}^D x_i = 1$. Therefore

$$\log D - \log a \leq \sigma^{D \rightarrow 1} \leq \log D. \quad (69)$$

The entropy grows asymptotically like $\log D + \mathcal{O}(1)$, independently of the exact tile fractions provided they remain bounded.

Large D phason elastic constants can also be calculated. Near the entropy maximum at $x_i = 1/D$,

$$K_i = \frac{\partial^2 \sigma}{\partial x_i^2} = -D. \quad (70)$$

Let $x_i = \frac{1}{D} + \delta x_i$, so that $\sigma = \sigma_{\max} - D \sum \delta x_i^2$. The average gradient of the function h (representing the one-dimensional membrane in the D -dimensional space) is characterized by the average angle ψ this membrane makes with the reference direction $(1, 1, \dots, 1)$. Specifically, $(\nabla h)^2 = \tan^2 \psi \simeq \psi^2$. Now,

$$1 - \frac{\psi^2}{2} \simeq \cos \psi = \left(D \sum_{i=1}^D x_i^2 \right)^{-1/2} \simeq 1 - \frac{D}{2} \sum_{i=1}^D \delta x_i^2. \quad (71)$$

Finally, $(\nabla h)^2 = D \sum \delta x_i^2$ and

$$\sigma^{D \rightarrow 1} \simeq \sigma_{\max} - \frac{K}{2} (\nabla h)^2, \quad (72)$$

where the phason elastic constant $K = 2$ is vanishingly small as compared to the entropy σ_{\max} .

2. $D \rightarrow 3$ tilings

Unlike the cases of $d = 1$ and $d = 2$, we have neither exact, nor extensive numerical information available for high codimension $d = 3$ tilings. Table II collects available data on $d = 3$ strain-free boundary tilings. For $D \leq 3$ the entropy vanishes. No data is available for $D = 5$. For $D = 4$ and 6, data is available from computer simulations^{44,45}. The $6 \rightarrow 3$ case⁴⁵ deals with rhombohedron tilings with icosahedral symmetry.

To estimate the large D limit, we insert oriented membranes into $d = 3$ tilings, as previously we inserted lines into $d = 2$ tilings. Membranes of like orientation are forbidden to cross. In the large D limit, we can neglect contact of like-oriented membranes and consider the statistics of a single membrane in generic high symmetry tilings. Let $M_D(\tau)$ denote the number of such membranes that can be inserted into tiling τ and \bar{M}_D be the arithmetic mean of this number. We find that the number of $D \rightarrow 3$ tilings is

$$B_D = \prod_{D'=3}^{D-1} \bar{M}_{D'}. \quad (73)$$

analogously to eq. (28). The entropy per tile is the logarithm of this number divided by the number of tiles.

We obtain an upper bound on the large D entropy of $d = 3$ tilings in a manner similar to our upper bound of $\log 2$ for $d = 2$. Recall 2^D is an upper bound on the number of directed paths in $d = 2$ tilings, and is actually realized only on special tilings in which the degree $Z = 4$ at all sites, with two incoming and two outgoing vertices. Similarly, the number of directed membranes may be maximal on a special tiling in which the coordination number and choice numbers are most homogeneous. This is the simple cubic tiling in which each vertex is six-fold coordinated. The membrane orientation should be in the plane perpendicular to the (111) axis. At each vertex there are 18 possible directed membrane configurations. This leads to $\bar{M}_D \leq 18^N$ membranes containing N rhombi, a substantial overestimate because many of these configurations force unique membrane structures nearby.

A true upper bound is

$$\bar{M}_D \leq e^{\sigma_{3 \rightarrow 2} N}, \quad \sigma^{D \rightarrow 3} \leq \sigma^{3 \rightarrow 2} \quad (74)$$

because the problem of the directed membrane on the simple cubic lattice is just the $3 \rightarrow 2$ tiling problem. This value is an upper bound because it neglects contacts, and because generic $D \rightarrow 3$ tilings will be less homogeneous than the simple cubic lattice and therefore the entropy lower.

3. $D \rightarrow D - 1$ tilings

In this section, we study the entropy of strain-free $D \rightarrow D - 1$ tilings where the D different tiles appear with the same fraction $1/D$ and we derive rigorous lower and upper bounds:

$$\frac{\log 2}{D} \leq \sigma^{D \rightarrow D-1} < \frac{3\sigma^{3 \rightarrow 2}}{D} \quad (75)$$

Note that the two prefactors $\log 2 \simeq 0.693$ and $3\sigma^{3 \rightarrow 2} \simeq 0.969$ are satisfactorily close and mutually consistent.

To derive the lower bound, we first notice that the elementary tiles of figure 3, namely hexagons and rhombic dodecahedrons, perfectly tile the entire two- and three-dimensional space, respectively. In fact, it is possible to tile any d -dimensional Euclidean space with the shadow P of a unit cube of dimension $D = d + 1$ projected along the $(1, 1, \dots, 1)$ direction. To understand this, consider all the unit cubes of a D -dimensional hypercubic lattice the centers of which belong to the diagonal hyperplane of equation $\sum x_i = 0$. Their projection along the $(1, 1, \dots, 1)$ direction is the desired tiling with the tile P . Now, such a polytope P can be tiled in two different ways with the D tiles of the $D \rightarrow D - 1$ tilings under consideration, as shown in figure 3, and independently of its neighbors. If we have a total of N tiles, we have N/D such polytopes, which provides $2^{N/D}$ different tilings. Thus the total number of tilings is bounded below by $2^{N/D}$, which leads to the lower bound (75) on $\sigma^{D \rightarrow D-1}$.

To understand the upper bound, we begin with the $4 \rightarrow 3$ case. In 3-dimensional tilings, we extend the notion of de Bruijn lines and define de Bruijn surfaces. The latter are connected sets of rhombohedral tiles which share a common face orientation. In $4 \rightarrow 3$ tilings, there are 4 families F_i of such surfaces, since there are 4 possible edge orientations $\hat{\mathbf{e}}_i^\parallel$. In d -dimensional tilings, there are $(d - 1)$ -dimensional surfaces defined similarly. Like in the two-dimensional case, two adjacent surfaces of a same family cannot cross but can have contacts.

Like in the previous subsection, such a surface in a $4 \rightarrow 3$ tiling can be put in one-to-one correspondence with a $3 \rightarrow 2$ tiling, just as in a $3 \rightarrow 2$ tiling, a de Bruijn line can be seen as a directed random walk on a square grid like a $2 \rightarrow 1$ tiling. Therefore if we do not take contacts between surfaces into account, a $4 \rightarrow 3$ tiling is a collection of independent $3 \rightarrow 2$ tilings, corresponding to all the de Bruijn surfaces of a given family. Of course, this approach will only provide an upper bound since contacts constraint the surfaces and reduce the entropy. Now the entropy of $3 \rightarrow 2$ tilings is known, and a fraction $3/4$ of the tiles of the original $4 \rightarrow 3$ tilings belong to the de Bruijn surfaces of the family under consideration. Therefore

$$\sigma^{4 \rightarrow 3} < \frac{3}{4} \sigma^{3 \rightarrow 2} = 0.242. \quad (76)$$

Now, we can iterate the same argument in any dimension, thus getting that

$$\sigma^{D \rightarrow D-1} < \frac{D-1}{D} \sigma^{D-1 \rightarrow D-2} < \frac{D-2}{D} \sigma^{D-2 \rightarrow D-3} < \dots < \frac{3}{D} \sigma^{3 \rightarrow 2}, \quad (77)$$

which leads to the upper bound eq. (75). The actual $4 \rightarrow 3$ entropy is strictly smaller than our bound (76), and its knowledge provides better upper bounds for larger D tilings. The best numerical estimate of this entropy is $\sigma^{4 \rightarrow 3} = 0.214 \pm 0.002$ [44], which leads to $\sigma^{D \rightarrow D-1} < 4\sigma^{4 \rightarrow 3}/D = (0.856 \pm 0.008)/D$ for $D \geq 4$, a noticeably better upper bound than (75). Similarly, the exact knowledge of any $D \rightarrow D - 1$ entropy would provide a better upper bound for the entropy of tilings of dimension larger than D .

V. CONCLUSION

This paper studied random tiling models in the limit of high rotational symmetry. We developed a mean-field theory for tilings based on the iterative construction of rhombus tilings introduced by de Bruijn⁴¹. The relevant quantity in this mean-field theory is the number of choices at each vertex, which is related to its coordination number (degree). The mean-field theory yields reasonable predictions for the configurational entropy of high symmetry, free boundary rhombus tilings in two dimensions, $\sigma_\infty^{MF} \simeq 0.598$, whereas the numerical value obtained by Monte Carlo numerical simulations is $\sigma_\infty \simeq 0.568$. We argue that high symmetry tilings become insensitive to phason strain, unlike finite symmetry tilings. In other words, phason elasticity vanishes at large codimension. In addition to the entropy and the phason elastic constants, we considered finite size corrections and correlation functions.

Our mean-field theory do not take into account spatial correlations which should modify slightly the entropy. For example, if a vertex has a low degree, it has less chance to be visited in the iterative process, which modifies the fixed point (36) and the entropy. Large degree vertices are more likely to be visited and to be split into two vertices

of lower degree. We expect them to be less numerous than in our calculation (see table IV), which accounts for the actual lower value of the entropy.

Our mean-field theory could be enhanced by inclusion of correlations. Instead of single vertices (with their arms and legs), one might instead study the statistics of pairs of vertices or even larger tiling patches and determine how these statistics evolve *via* the iterative process, when they are split into two pieces by a path going through them. It would also be useful to predict how the spatial correlations calculated in the paper perturb the mean-field entropy.

A second paper³⁵ follows this one and presents the numerical Monte Carlo study of large codimension tilings. In particular, it is demonstrated in this paper that in such tilings, the thermodynamic limit is restored: fixed boundaries do not result in the lowering of the entropy like in finite codimension cases.

ACKNOWLEDGMENTS

We thank Chris Henley and Pavel Kalugin for useful discussions. This research is supported in part by the National Science Foundation under grants DMR-0111198 and INT-9603372 and by the CNRS.

APPENDIX A: CONSTRUCTION OF THE HEIGHT FUNCTION

This appendix constructs⁴⁰ the parallel and perpendicular spaces ($\mathcal{E}^{\parallel} = \mathbf{R}^2$ and $\mathcal{E}^{\perp} = \mathbf{R}^{D-2}$) for $D \rightarrow 2$ tilings as well as the mapping $h : \mathcal{E}^{\parallel} \rightarrow \mathcal{E}^{\perp}$. We embed these spaces in the D -dimensional hyperspace \mathbf{R}^D . Let the unit vectors $\{\hat{\mathbf{e}}_i\}$ be an orthonormal basis for \mathbf{R}^D . Their normalized projections into \mathcal{E}^{\parallel} and \mathcal{E}^{\perp} will be denoted, respectively, by $\hat{\mathbf{e}}_i^{\parallel}$ and $\hat{\mathbf{e}}_i^{\perp}$. Our first task is to represent these projections in the hyperspace basis.

We define the two-dimensional “parallel” space \mathcal{E}^{\parallel} by its orthonormal basis

$$\begin{aligned}\hat{x}^{\parallel} &= \sqrt{\frac{2}{D}} \sum_{j=0}^{D-1} \hat{\mathbf{e}}_j \cos\left(\frac{\pi j}{D}\right) \\ \hat{y}^{\parallel} &= \sqrt{\frac{2}{D}} \sum_{j=0}^{D-1} \hat{\mathbf{e}}_j \sin\left(\frac{\pi j}{D}\right).\end{aligned}\tag{A1}$$

Given the basis for \mathcal{E} we define the projection operator P_{\parallel} by $P_{\parallel}(u) \equiv (\hat{x}^{\parallel} \cdot u)\hat{x}^{\parallel} + (\hat{y}^{\parallel} \cdot u)\hat{y}^{\parallel}$ and its complement $P_{\perp} = 1 - P_{\parallel}$. The parallel space vectors $\hat{\mathbf{e}}_i^{\parallel}$ are the projections of suitably scaled hyperspace basis vectors,

$$\hat{\mathbf{e}}_i^{\parallel} \equiv P_{\parallel}(s_{\parallel} \hat{\mathbf{e}}_i).\tag{A2}$$

Note that they form a regular fan

$$\hat{\mathbf{e}}_i^{\parallel} = \hat{x}^{\parallel} \cos\left(\frac{\pi i}{D}\right) + \hat{y}^{\parallel} \sin\left(\frac{\pi i}{D}\right).\tag{A3}$$

By a “regular fan” we mean a collection of equally spaced vectors arranged in the upper half plane. The union of these vectors and their negatives forms a $2D$ -fold symmetric star. We set the scale factor $s_{\parallel} = \sqrt{D/2}$ to normalize $\hat{\mathbf{e}}_i^{\parallel}$ in eq. (A3).

The $(D-2)$ -dimensional “perpendicular” space \mathcal{E}^{\perp} is the complement in \mathbf{R}^D of \mathcal{E}^{\parallel} . Consider the projection of the scaled hyperspace vector $s_{\perp} \hat{\mathbf{e}}_i$ into \mathcal{E}^{\perp} , which we can express as

$$\hat{\mathbf{e}}_i^{\perp} \equiv P_{\perp}(s_{\perp} \hat{\mathbf{e}}_i) = s_{\perp}(\hat{\mathbf{e}}_i - P_{\parallel} \hat{\mathbf{e}}_i).\tag{A4}$$

Its magnitude can be found from

$$\|P_{\perp} s_{\perp} \hat{\mathbf{e}}_i\|^2 = s_{\perp}^2 (1 + \|P_{\parallel} \hat{\mathbf{e}}_i\|^2 - 2 \hat{\mathbf{e}}_i \cdot P_{\parallel} \hat{\mathbf{e}}_i) \equiv 1.\tag{A5}$$

We evaluate $\|P_{\parallel} \hat{\mathbf{e}}_i\|^2 = 1/s_{\parallel}^2 = 2/D$ from eq. (A2), and we evaluate $\hat{\mathbf{e}}_i \cdot P_{\parallel} \hat{\mathbf{e}}_i = \sqrt{2/D} \hat{\mathbf{e}}_i \cdot \hat{\mathbf{e}}_i^{\parallel} = 2/D$ from eq. (A3) together with eq. (A1). Then eq. (A5) yields $s_{\perp} = 1/\sqrt{1 - 2/D}$. The following result will also be useful: if $i \neq j$ then

$$\hat{\mathbf{e}}_i^\perp \cdot \hat{\mathbf{e}}_j^\perp = -\frac{2}{D-2} \hat{\mathbf{e}}_i^\parallel \cdot \hat{\mathbf{e}}_j^\parallel. \quad (\text{A6})$$

Indeed, $\hat{\mathbf{e}}_i \cdot \hat{\mathbf{e}}_j = \delta_{ij} = \hat{\mathbf{e}}_i^\parallel \cdot \hat{\mathbf{e}}_j^\parallel / s_\parallel^2 + \hat{\mathbf{e}}_i^\perp \cdot \hat{\mathbf{e}}_j^\perp / s_\perp^2$.

Every vertex v in a rhombus tiling occupies a position of the form

$$\mathbf{r}_\parallel(v) = \sum_{i=1}^D \mathcal{R}_i(v) \hat{\mathbf{e}}_i^\parallel \in \mathcal{E}^\parallel \quad (\text{A7})$$

where the coefficients \mathcal{R}_i are integers. To find the values of \mathcal{R}_i for vertex v , choose any vertex as the origin for \mathcal{E}^\parallel , then follow a path of rhombus edges from the origin to v . Adding to (or subtracting from) \mathcal{R}_i for each edge $\hat{\mathbf{e}}_i^\parallel$ along the path yields the values of $\mathcal{R}_i(v)$. The perpendicular space position of that vertex is defined as

$$h(\mathbf{r}_\parallel) = h(v) = \sum_{i=1}^D \mathcal{R}_i(v) \hat{\mathbf{e}}_i^\perp \in \mathcal{E}^\perp. \quad (\text{A8})$$

Values of $h(\mathbf{r})$ for \mathbf{r} in the interior of a tile can be defined using linear interpolation on the values just defined for tile vertices.

The equation of a flat (strain-free) tiling, or of a locally flat tiling after coarse-graining is defined by D vectors $\mathbf{m}_i \in \mathcal{E}^\parallel$ such that

$$\mathcal{R}_i(v) = \mathbf{m}_i \cdot \mathbf{r}_\parallel, \quad (\text{A9})$$

the above equality meaning that $\mathcal{R}_i(v)$ is the closest integer to the right-hand side quantity. Then the $(D-2) \times 2$ phason gradient tensor $\mathbf{E} = \nabla_\parallel h(\mathbf{r}_\parallel)$ is

$$\mathbf{E} = \sum_{i=1}^D \hat{\mathbf{e}}_i^\perp \otimes \mathbf{m}_i, \quad (\text{A10})$$

where $\hat{\mathbf{e}}_i^\perp \otimes \mathbf{m}_i$ is a the tensor product of the *column* vector $\hat{\mathbf{e}}_i^\perp$ and the *line* vector \mathbf{m}_i .

¹ D. Shechtman, *et al.*, *Phys. Rev. Lett.* **53**, 1951 (1984).

² D. Levine, P.J. Steinhardt, *Phys. Rev. Lett.* **53**, 2477 (1984).

³ R. Penrose, *Bull. Inst. Math. Appl.* **10**, 226 (1974).

⁴ V. Elser, *Phys. Rev. Lett.* **54**, 1730 (1985).

⁵ C.L. Henley, in *Quasicrystals, the State of the Art*, Ed. D.P. Di Vincenzo, P.J. Steinhardt (World Scientific, 1991), 429.

⁶ M. Widom, K.J. Strandburg, R.H. Swendsen, *Phys. Rev. Lett.* **58**, 706 (1987).

⁷ F. Lançon, L. Billard, P. Chaudhari, *Europhys. Lett.* **2**, 625 (1986).

⁸ H.-C. Jeong, P.J. Steinhardt, *Phys. Rev. Lett.* **73**, 1943 (1994); K. Ingersent, P.J. Steinhardt, *Phys. Rev. Lett.*, **64**, 2034 (1990).

⁹ M. Widom, in *Quasicrystals*, eds. M.V. Jaric, S. Lundqvist (World Scientific, 1990), 337.

¹⁰ R. Mosseri, F. Bailly, *Int. J. Mod. Phys. B*, Vol 7, **6&7**, 1427 (1993).

¹¹ N. Destainville, R. Mosseri, F. Bailly, *J. Stat. Phys.* **87**, Nos 3/4, 697 (1997).

¹² N. Destainville, R. Mosseri, F. Bailly, *J. Stat. Phys.* **102**, 147 (2001).

¹³ *Oriented Matroids*, A. Björner, M. Las Vergnas, B. Sturmfels, N. White, G.M. Ziegler (Cambridge University Press, 1993).

¹⁴ R. Kenyon, *Algorithmica* **9**, 382 (1993).

¹⁵ S. Elnitsky, *J. Combinatorial Theory A* **77**, 193–221 (1997).

- ¹⁶ *Tilings of zonotopes: Discriminantal arrangements, oriented matroids, and enumeration*, G.D. Bailey, Ph. D. Thesis (Univ. of Minnesota, 1997).
- ¹⁷ H. Cohn, M. Larsen, J. Propp, *New York J. of Math.* **4**, 137 (1998).
- ¹⁸ H. Cohn, R. Kenyon, J. Propp, *J. of the AMS* **14**, 297 (2001).
- ¹⁹ R. Cerf, R. Kenyon, *Comm. Math. Phys.* **222**, 147 (2001).
- ²⁰ M. Latapy, *RAIRO-Theor. Inf. Appl.* **36**, 389 (2002).
- ²¹ H.W.J. Blöte, H.J. Hilhorst, *J. Phys. A* **15**, L631 (1982).
- ²² M. Widom *Phys. Rev. Lett.* **70**, 2094 (1993); P. Kalugin *J. Phys. A* **27**, 3599 (1994); J. de Gier, B. Nienhuis, *Phys. Rev. Lett.* **76**, 2918 (1996); J. de Gier, B. Nienhuis, *J. Phys. A* **31**, 2141 (1998).
- ²³ D.M. Knuth, Axioms and Hulls, in *Lect. Notes in Computer Sci.* **606**, 35 (1992).
- ²⁴ M. Widom, N. Destainville, R. Mosseri, F. Bailly, in *Proceedings of the 6th International Conference on Quasicrystals*, (World Scientific, Singapore, 1997).
- ²⁵ M.V. Jaric and S.L. Johnson, *Phys. Lett. A* **219**, 238 (1996).
- ²⁶ K.J. Strandburg, L.-H. Tang and M.V. Jaric *Phys. Rev. Lett.* **63**, 314 (1989); L.J. Shaw, V. Elser, C.L. Henley, *Phys. Rev. B* **43**, 3423 (1989); L.-H. Tang, *Phys. Rev. Lett.* **64**, 2390 (1990); M. Oxborow and C.L. Henley, *Phys. Rev. B* **48**, 6966 (1993); F. Gähler, Proc. ICQ5 236 (1995); D. Joseph and M. Baake, *J. Phys. A* **29**, 6709 (1996).
- ²⁷ M. Widom, D.P. Deng and C.L. Henley *Phys. Rev. Lett.* **63**, 310 (1989); L.J. Shaw and C.L. Henley, *J. Phys. A* **24**, 4129 (1991); M.E.J. Newman and C.L. Henley, *Phys. Rev. B* **52**, 6386 (1995).
- ²⁸ *Statistical Field Theory*, Vol 1, C. Itzykson, J.-M. Drouffe (Cambridge Monographs on Mathematical Physics, 1992).
- ²⁹ V.E. Korepin, F. Gähler and J. Rhyner, *Acta Cryst. A* **44**, 667 (1988).
- ³⁰ J.E.S. Socolar, P.J. Steinhardt and D. Levine, *Phys. Rev. B* **32**, 5547 (1985).
- ³¹ D.A. Rabson, N.D. Mermin, D.S. Rokhsar and D.C. Wright, *Rev. Mod. Phys.* **63**, 699 (1991).
- ³² *Random graphs*, B. Bollobas (Academic Press, New York, 1985).
- ³³ J. Vidal, N. Destainville, R. Mosseri, to appear in *Phys. Rev. B* **68** (2003).
- ³⁴ N. Destainville, M. Widom, R. Mosseri, F. Bailly, *Mat. Sci. Eng. A* **294**, 409, (2000).
- ³⁵ M. Widom, N. Destainville, R. Mosseri, F. Bailly, following paper “Random tilings with high symmetry: II. Monte Carlo simulation”.
- ³⁶ V. Elser *J. Phys. A* **17**, 1509 (1984).
- ³⁷ G.H. Wannier, *Phys. Rev.* **79**, 357 (1950); *Phys. Rev. B* **7** 5017 (E, 1973).
- ³⁸ N. Destainville, *J. Phys. A: Math. Gen.* **31**, 6123 (1998).
- ³⁹ *Regular Polytopes*, H.S.M. Coxeter (Dover, 1973).
- ⁴⁰ W. Li, H. Park, M. Widom, *J. Stat. Phys.* **66**, 1 (1992).
- ⁴¹ N.G. de Bruijn, *Ned. Akad. Wetensch. Proc.* **A84**, 39 (1981); *J. Phys. France* **47**, C3-9 (1986).
- ⁴² J.E.S. Socolar, P.J. Steinhardt, D. Levine, *Phys. Rev. B* **32**, No 8, 5547 (1985).
- ⁴³ F. Gähler, J. Rhyner, *J. Phys. A: Math. Gen.* **19**, 267 (1986).
- ⁴⁴ M. Widom, R. Mosseri, N. Destainville, F. Bailly, *J. Stat. Phys.* **109**, 945 (2002).
- ⁴⁵ K.J. Strandburg, *Phys. Rev. B* **44**, 4644 (1991).

TABLE I. $D \rightarrow 2$ strain-free rhombus tiling entropies.

D	2	3	4	5	∞
σ	0	0.323	0.434	0.481	0.568

TABLE II. $D \rightarrow 3$ strain-free rhombohedron tiling entropies.

D	3	4	5	6	∞
σ	0	0.214	NA	0.24	< 0.323

TABLE III. Entropy estimates in the large D limit.

Value	Method	Reference
0.693	exact upper bound	eq. (30)
0.6	extrapolated exact values	Ref. [²⁴]
0.598	mean-field theory	eq. (37)
0.568	simulation	Ref. [³⁵]

 TABLE IV. The first values of the limiting distribution $\pi(N_c)$, obtained both in the mean-field approximation eq. (36) and numerically, by Monte Carlo simulations (from paper II³⁵).

N_c	1	2	3	4	5
$\pi(N_c)$ (Mean-field)	0.30	0.45	0.19	0.04	0.007
$\pi(N_c)$ (Numerical)	0.26	0.51	0.21	0.03	0.001